Electronic Supplementary Material (ESI) for Journal of Materials Chemistry A.

Supporting Information.

Bifunctional oxygen electrocatalysis on ultra-thin Co_9S_8/MnS carbon nanosheets for all-solid state zinc-air batteries

Jiacheng Li, Wanqing Li, Hongwei Mi*, Yongliang Li, Libo Deng, Qianling Zhang, Chuanxin He, Xiangzhong Ren*

College of Chemistry and Environmental Engineering, International Joint Research Center for Molecular Science, Shenzhen University, Shenzhen, Guangdong 518060, P.R. China

Corresponding author:

Xiangzhong Ren, E-mail: renxz@szu.edu.cn, Tel/Fax: +86-755-26558134

Hongwei Mi, E-mail: milia807@szu.edu.cn, Tel/Fax: +86-755-26538657

1. Sample characterizations

The characterizations were carried out as previous work.[1] The transmission electron microscopy (TEM, FEI Tecnai G2 F30) and field emission scanning electron microscopy (FESEM, JEOL JSM-7800F) are applied to observe the morphology and microstructure of specific materials. Additionally, the field emission transmission electron microscope (TEM, JEOL JEM-F200) was used to detected EDS mapping of prepared samples. The phase existence and crystal plane were investigated by X-ray diffraction (XRD) on a PANalytical/Empyrean with Cu Kα radiation. Raman spectra were obtained using the Renishaw/INVIA REFLEX spectrometer. N_2 adsorption-desorption isotherms were measured by the BELSORP-max instrument. The specific surface area and pore size distribution were demonstrated by Brunauer-Emmett-Teller (BET) theory and nonlocal density functional theory (NLDFT), respectively. X-ray photoelectron spectroscopy (XPS) measurements were performed on a K-Alpha$^+$ spectrometer equipped with a monochromic Al X-ray source.

2. Electrochemical measurement

2.1 Preparation of the working electrode

The preparation was complished as previous works.[2, 3] 1 mg of the sample was dispersed into 0.3 mL of ethanol with 8 μL 5 wt% Nafion, and the mixture was sonicated for 1 h. Afterward, 20 μL of the mentioned solution divided into 5μL for 4 times was dropped on a glassy carbon rotating ring disk electrode disk (Adisk=0.126 cm^2, Aring=0.188 cm^2, Φ=4 mm, inner/outer-ring diameter=5.0/7.0 mm) from BAS Inc. The mass loading of the catalyst is 0.398 $mg{\cdot}cm^{-2}$.

2.2 Electrochemical evaluations

A three-electrode system, where an Ag/AgCl electrode saturated with KCl was used as the reference electrode and a Pt wire was for the counter electrode, was applied to perform the presented tests. All tests were taken at the temperature of 25 °C and all tested values of potential were adjusted according to the reversible hydrogen electrode (RHE). All the tests were accomplished in 1 mol·L^{-1} KOH with O_2 saturated. With a scan rate of 5 mV·s^{-1} and at different speeds of 400, 600, 900, 1200, and 1600 rpm, the linear sweep voltammogram (LSV) test was conducted. From 0.2-1.2 V and with a scan rate of 100 mV·s^{-1}, the durability of CV testing test was carried out for ORR, while for OER the potential gap is from 1.2-1.9 V. During the i-t stability test of ORR, 1 mL CH_3OH was introduced into the electrolyte to measure the anti-toxicity ability. Commercialized 20 wt% Pt/C was used as the standard for ORR performance, meanwhile, Ir/C was for OER. According to the CV test from 0.99-1.99 V, the electrochemical double-layer capacitance (C_{dl}) of the electrocatalyst was measured.

2.3 Calculation of electron transfer number (n) and %HO^{2-} for the oxygen reduction reaction

According to the Koutecky-Levich (K-L) equations, which was given as follow, the electron transfer number (n) will be well explored:

$$\frac{1}{J}=\frac{1}{B\omega^{1/2}}+\frac{1}{J_K} \qquad (1)$$

$$B=0.2nFC_0{D_0}^{2/3}\nu^{-1/6} \qquad (2)$$

$$J_K=nFKC_0 \qquad (3)$$

In the above equations, J represents the measured current density, while J_K is the kinetic limiting current density. ω is used to describe the angular velocity of the disk, which can be calculated from ω = 2πN, where N is the linear rotation speed. Using n to note the electrons transfer number. F is the Faraday constant equals to 96485 C·mol^{-1} approximately. The bulk concentration of O_2 was considered as C_0, while the kinematic viscosity of the electrolyte is ν. Also, k is the electron transfer rate constant, and D_0 is the diffusion coefficient of O_2 in the electrolyte. While the rotation speed is expressed in rpm, 0.2 as the constant is adopted. In this paper, the potentials according to K-L equations to obtain the electron transfer number from the LSV curves are 0.35, 0.40, 0.45, and 0.50V.

The electron transfer number (n) and the corresponding peroxide yield (HO^{2-} in alkaline solution) can also be determined based on the disk and ring currents using the following equations:

$$n = 4 \times \frac{I_{disk}}{I_{disk} + \frac{I_{ring}}{N}} \qquad (4)$$

$$peroxide\% = 100 \times \frac{2\frac{I_{ring}}{N}}{I_{disk} + \frac{I_{ring}}{N}} \qquad (5)$$

In the above equations, I_{disk} and I_{ring} respectively represent the Faraday disk and ring currents. The collection efficiency of the ring electrode, 0.43 here, is described as the constant of N. The disk electrode was scanned at a rate of 5 $mV \cdot s^{-1}$, and the ring potential was constant at 0.5 V.

2.4 Zinc-Air battery tests

The performance of zinc-air batteries was evaluated in self-made batteries. The air cathode is 1 cm^2 (1 cm × 1 cm) gas diffusion layers with a dispersion of specific electrocatalyst, while the anode is zinc plates. For the electrolyte, the mixed solution of 6.0 M KOH with 0.2 M $Zn(Ac)_2$ was used. As a comparison, 1 mg of Pt/C and 1 mg of Ir/C were mechanically mixed as references. The charging process and discharging process were respectively 10 min in cycling durability tests of the zinc-air batteries, which was achieved by the LAND battery test station (CT2001A). The test programs of the all-solid-state zinc-air batteries are the same as the aqueous zinc-air batteries.

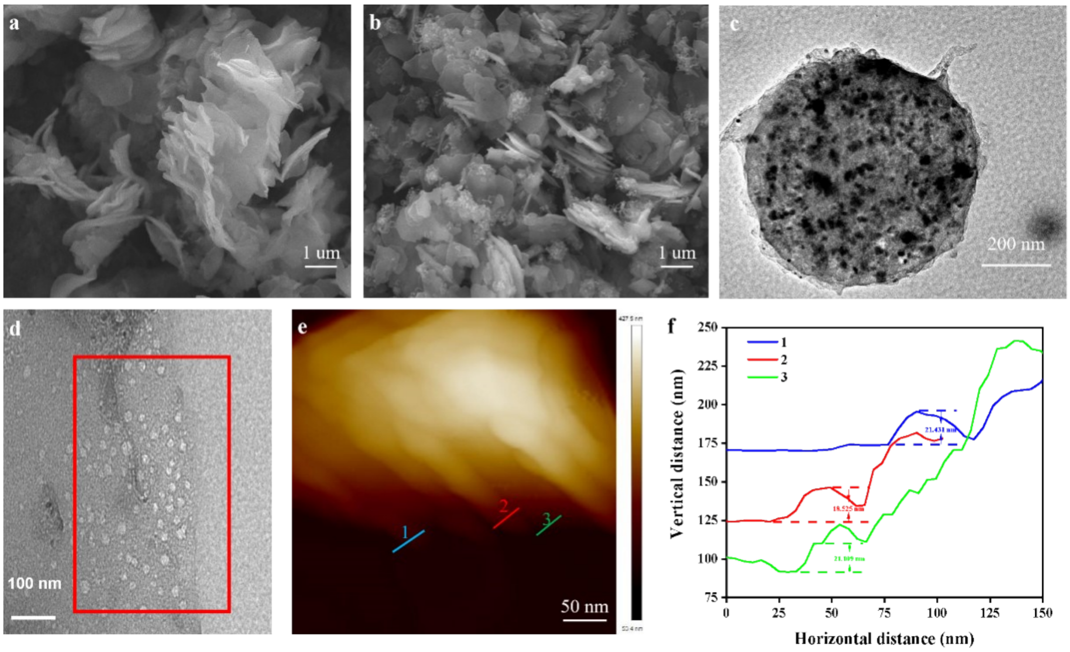

Fig.S1 SEM image of (a) MnS-USNC and (b) Co_9S_8-USNC; (c-d) TEM images of Co_9S_8/MnS-USNC; (e) AFM height image and (f) horizontal and vertical distance curve of Co_9S_8/MnS-USNC at different points

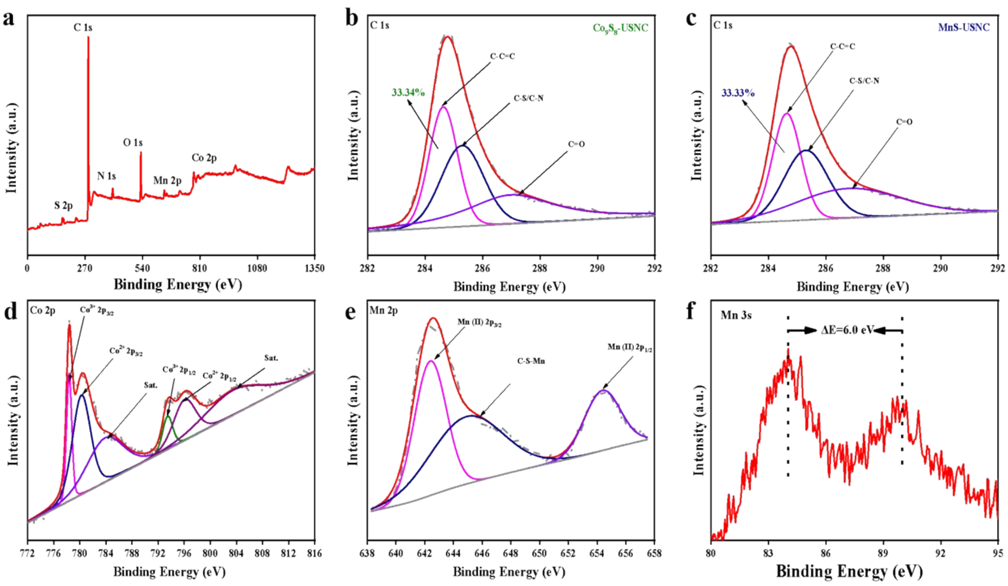

Fig.S2 (a) XPS survey of Co_9S_8/MnS-USNC; C 1s of (b) Co_9S_8-USNC and (c) MnS-USNC; (d) Co 2p of Co_9S_8-USNC; (e) Mn 2p and (f) Mn 3s of Co_9S_8/MnS-USNC

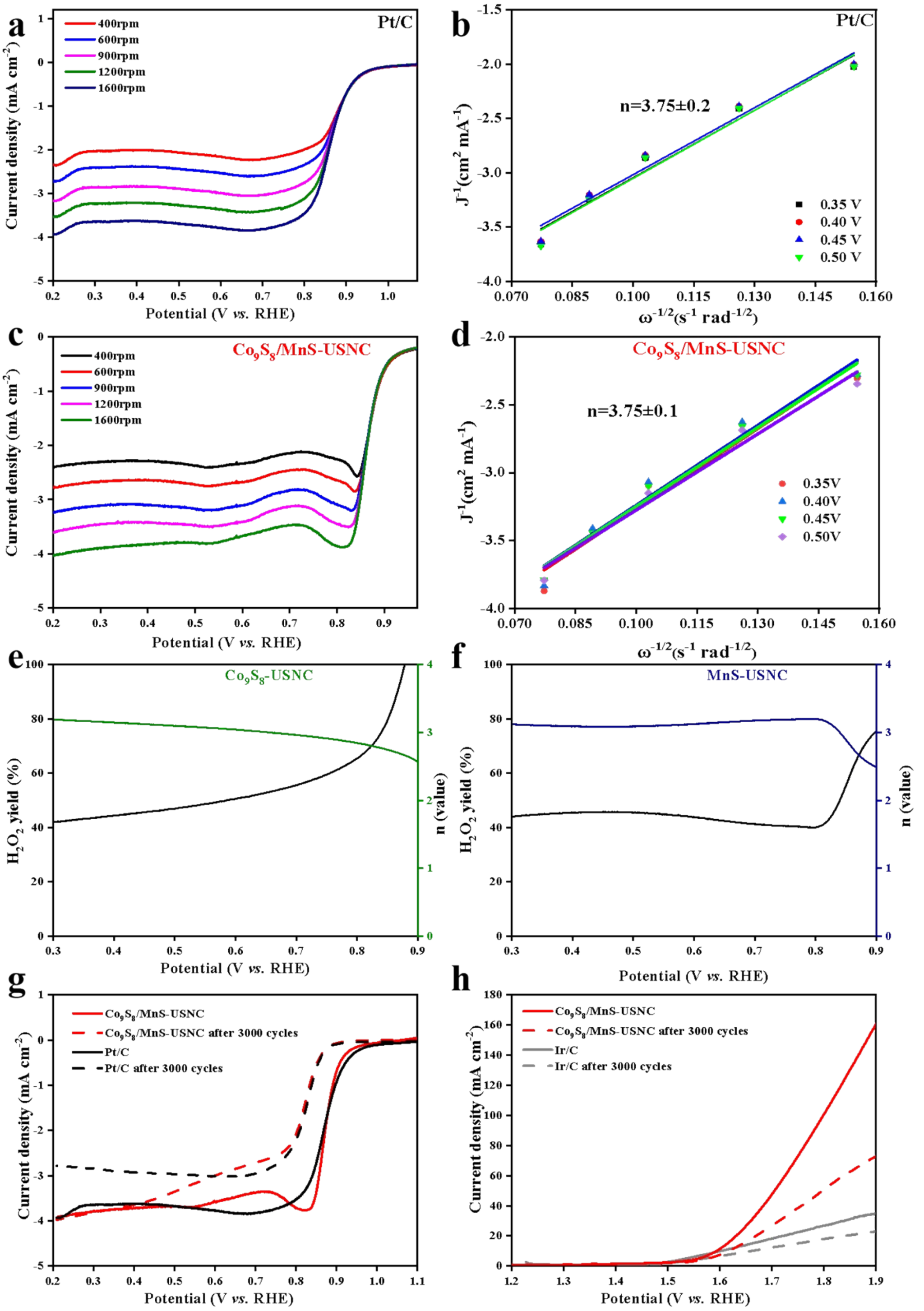

Fig.S3 LSV curves of (a) Pt/C and (c) Co_9S_8/MnS-USNC at different rotation speed and calculated K-L plot of (b) Pt/C and(d) Co_9S_8/MnS-USNC; H_2O_2 yield and electron transfer number of (e) Co_9S_8-USNC and (f) MnS-USNC; (g) LSV curves obtained before and after 3000 cycles CV test of

Pt/C and Co_9S_8/MnS-USNC; (h) initial LSV curves and the LSV curves obtained after 3000 cycles of Ir/c and Co_9S_8/MnS-USNC.

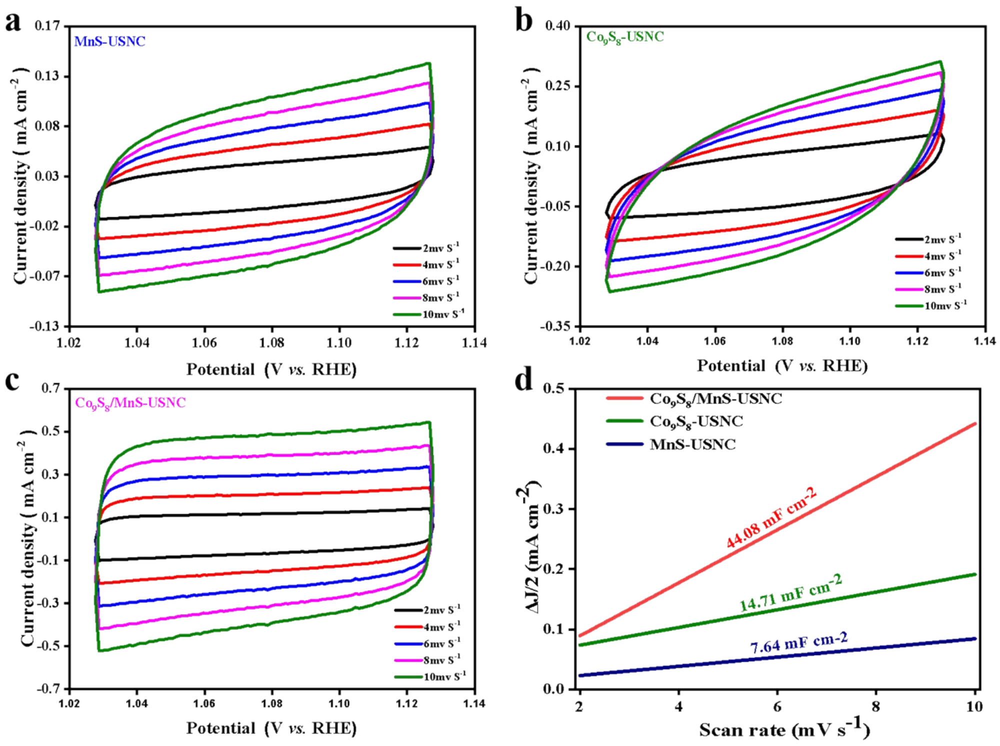

Fig.S4 Cyclic voltammograms from 1.03 to 1.13 V *vs.* RHE of (a) MnS-USNC, (b) Co_9S_8-USNC, and (c) Co_9S_8/MnS-USNC and (h) the calculated C_{dl} values of Co_9S_8/MnS-USNC, MnS-USNC, and Co_9S_8-USNC.

Table S1. The horizontal and vertical distance of Co_9S_8/MnS-USNC at different points

Pair	Horizontal Distance (nm)	Vertical Distance (nm)
1	13.594	21.431
2	16.464	18.525
3	12.467	21.109

Table S2. Atomic % of S 2p, C 1s, N 1s, O 1s, Co 2p, and Mn 2p

Name	Peak BE	Atomic %
S 2p	163.63	3.69
C 1s	284.8	78.69
N 1s	399.39	5.14
O 1s	531.95	9.6
Mn 2p	641.95	0.89
Co 2p	781.12	2

Table S3. The catalytic performance of various Co or/and Mn-based electrocatalysts from kinds of literature.

Electrocatalyst	ORR		OER	ΔE	Literature
	E_{onset} (V)	$E_{1/2}$ (V)	$E_{j=10}$ (V)	($E_{j=10}$-$E_{1/2}$) (V)	
Co_9S_8/MnS-USNC	**1.00**	**0.90**	**1.59**	**0.69**	**This work**
Co_9S_8@Co_3O_4	/	/	1.40*	/	4
0.5-Co_9S_8@N-C	0.85*	0.83	/	/	5
Co_9S_8-NSHPCNF	0.85*	0.82	1.58*	0.76	6
Co_9S_8/CS-800	0.95	0.82	1.60	0.78	7
Co_9S_8@MoS_2	0.90*	0.85*	1.58*	0.73*	8
N-Co_9S_8/G	0.94	0.82*	1.62*	0.80	9
NC-FeCoNiMn_4	0.94	0.86	1.57	0.71	10
Fe_3O_4@Co_9S_8/rGO-2	/	/	1.60*	/	11
Co_9S_8 HMs-140/C	0.95	0.82	1.63*	0.81*	12
$Mn_{0.5}(Fe_{0.3}Ni_{0.7})_{0.5}O_x$/MWCNTs-$O_x$	/	0.81	1.57	0.76	13
Co_9S_8/NSG-700	0.92	0.79	1.61	0.82	14
Co_9S_8@N-S-HPC	0.95	0.85*	/	/	15
IOSHs-NSC-Co_9S_8	0.85*	0.82	1.64*	0.82*	16
Co_9S_8/P@CS-1:2	/	/	1.46*	/	17

* Not mentioned in the literature but derived from the LSV curves and calculations.

Table S4. The survey of the performance of rechargeable zinc-air batteries with various electrocatalysts.

Electrocatalyst	Peak power density ($mW\ cm^{-2}$)	Stability	Literature
Co_9S_8/MnS-USNC	**146**	**600 h at 5 mA cm^{-2}**	**This work**
Co_9S_8-NSHPCNF	113	20000 min at 2 mA cm^{-2} 4000 min at 10 mA cm^{-2}	[6]
Co_9S_8@MoS_2	/	20 h at 10 mA cm^{-2}	[8]
Co_9S_8/NSG-700	274	138 h at 10 mA cm^{-2}	[14]
IOSHs-NSC-Co_9S_8	133	80 h at 10 mA cm^{-2}	[16]
Co_9S_8/P@CS-1:2	142	350 h at 5 mA cm^{-2}	[17]
Co/MnO@N,S-C NT/NFs + RuO_2	120.7	500h at 5 mA cm^{-2}	[18]

Table S5. The survey of the performance of rechargeable all-solid-state zinc-air batteries with various electrocatalysts.

Electrocatalyst	**Peak power density ($mW\ cm^{-2}$)**	**Stability**	**Literature**
Co_9S_8/MnS-USNC	**79**	**18 h at 5 $mA\ cm^{-2}$**	**This work**
NPC/FeCo@NCNT	65	40 cycles at 1 $mA\ cm^{-2}$	[19]
FeCo/Se-CNT	37.5	20 h at 5 $mA\ cm^{-2}$	[20]
Co-NDC	45.9	20c at 2 $mA\ cm^{-2}$	[21]
IOSHs-NSC-Co_9S_8	/	35h at 5 $mA\ cm^{-2}$	[16]
Co_3O_4/N-CNT aerogel	/	20 h at 2 $mA\ cm^{-2}$	[22]

REFERENCES

1. Y. Sun, Y. Guan, X. Wu, W. Li, Y. Li, L. Sun, H. Mi, Q. Zhang, C. He and X. Ren, *Nanoscale*, 2021, **13**, 3227-3236.
2. Y. Guan, Y. Li, S. Luo, X. Ren, L. Deng, L. Sun, H. Mi, P. Zhang and J. Liu, *Appl. Catal. B,* 2019, **256**, 117871.
3. Y. Guan, N. Li, Y. Li, L. Sun, Y. Gao, Q. Zhang, C. He, J. Liu and X. Ren, *Nanoscale*, 2020, **12**, 14259-14266.
4. S. Deng, S. Shen, Y. Zhong, K. Zhang, J. Wu, X. Wang, X. Xia and J. Tu, *J. Energy Chem.*, 2017, **26**, 1203-1209.
5. Z. Wu, J. Wang, M. Song, G. Zhao, Y. Zhu, G. Fu and X. Liu, *ACS Appl. Mater.*, 2018, **10**, 25415-25421.
6. W. Peng, Y. Wang, X. Yang, L. Mao, J. Jin, S. Yang, K. Fu and G. Li, *Appl. Catal. B*, 2020, **268**, 118437.
7. W. Li, Y. Li, H. Wang, Y. Cao, H. Yu and F. Peng, *Electrochim. Acta*, 2018, **265**, 32-40.
8. J. Bai, T. Meng, D. Guo, S. Wang, B. Mao and M. Cao, *ACS Appl. Mater.*, 2018, **10**, 1678-1689.
9. S. Dou, L. Tao, J. Huo, S. Wang and L. Dai, *Energy Environ. Sci.*, 2016, **9**, 1320-1326.
10. S. Gupta, S. Zhao, X. X. Wang, S. Hwang, S. Karakalos, S. V. Devaguptapu, S. Mukherjee, D. Su, H. Xu and G. Wu, *ACS Catal.*, 2017, **7**, 8386-8393.
11. J. Yang, G. Zhu, Y. Liu, J. Xia, Z. Ji, X. Shen and S. Wu, *Adv. Funct. Mater.*, 2016, **26**, 4712-4721.
12. Y. Zhang, S. Chao, X. Wang, H. Han, Z. Bai and L. Yang, *Electrochim. Acta*, 2017, **246**, 380-390.
13. D. M. Morales, M. A. Kazakova, S. Dieckhöfer, A. G. Selyutin, G. V. Golubtsov, W. Schuhmann and J. Masa, *Adv. Funct. Mater.*, 2019, **30**, 1905992.
14. Q. Shao, J. Liu, Q. Wu, Q. Li, H.-g. Wang, Y. Li and Q. Duan, *Nano-Micro Lett.*, 2019, **11**, 4.
15. S. Zhang, D. Zhai, T. Sun, A. Han, Y. Zhai, W.-C. Cheong, Y. Liu, C. Su, D. Wang and Y. Li, *Appl. Catal. B*, 2019, **254**, 186-193.
16. K. Tang, C. Yuan, Y. Xiong, H. Hu and M. Wu, *Appl. Catal. B*, 2020, **260**, 118209.
17. W. Li, Y. Li, H. Fu, G. Yang, Q. Zhang, S. Chen and F. Peng, *Chem. Eng. J.*, 2020, **381**, 122683.
18. Q. Zhou, S. Hou, Y. Cheng, R. Sun, W. Shen, R. Tian, J. Yang, H. Pang, L. Xu, K. Huang and Y. Tang, *Appl. Catal. B*, 2021, **295**, 120281.
19. X. Hao, Z. Jiang, B. Zhang, X. Tian, C. Song, L. Wang, T. Maiyalagan, X. Hao and Z. J. Jiang, *Adv. Sci.*, 2021, **8**, 2004572.
20. H. Zhang, M. Zhao, H. Liu, S. Shi, Z. Wang, B. Zhang, L. Song, J. Shang, Y. Yang, C. Ma, L. Zheng, Y. Han and W. Huang, *Nano Lett.*, 2021, **21**, 2255-2264.
21. Z. Chen, Q. Wang, X. Zhang, Y. Lei, W. Hu, Y. Luo and Y. Wang, *Sci. Bull.*, 2018, **63**, 548-555.
22. S. Zeng, H. Chen, H. Wang, X. Tong, M. Chen, J. Di and Q. Li, *Small*, 2017, **13**, 1700518.